Creation of half-metallic f-orbital Dirac fermion with superlight elements in orbital-designed molecular lattice

Bin Cui,[1,2] Bing Huang,[3,2,*] Chong Li,[4,2] Xiaoming Zhang,[1,2] Kyung-Hwan Jin,[2] Lizhi Zhang,[2] Wei Jiang,[2] Desheng Liu,[1,5] and Feng Liu[2,6,†]

[1]*School of Physics, Shandong University, Jinan 250100, China*

[2]*Department of Materials Science and Engineering, University of Utah, Salt Lake City, Utah 84112, USA*

[3]*Beijing Computational Science Research Center, Beijing 100193, China*

[4]*School of Physics and Engineering, Zhengzhou University, Zhengzhou, 450001, China*

[5]*Department of Physics, Jining University, Qufu 273155, China*

[6]*Collaborative Innovation Center of Quantum Matter, Beijing 100084, China*

(Received 10 January 2017; published 23 August 2017)

Magnetism in solids generally originates from the localized d or f orbitals that are hosted by heavy transition-metal elements. Here, we demonstrate a mechanism for designing a half-metallic f-orbital Dirac fermion from superlight sp elements. Combining first-principles and model calculations, we show that bare and flat-band-sandwiched (FBS) Dirac bands can be created when C_{20} molecules are deposited into a two-dimensional hexagonal lattice, which are composed of f-molecular orbitals (MOs) derived from sp-atomic orbitals (AOs). Furthermore, charge doping of the FBS Dirac bands induces spontaneous spin polarization, converting the system into a half-metallic Dirac state. Based on this discovery, a model of a spin field effect transistor is proposed to generate and transport 100% spin-polarized carriers. Our finding illustrates a concept to realize exotic quantum states by manipulating MOs, instead of AOs, in orbital-designed molecular crystal lattices.

DOI: 10.1103/PhysRevB.96.085134

I. INTRODUCTION

Magnetic ordering in solids is generally associated with heavy elements, and tremendous efforts have been devoted in the past decades to finding transition-metal (TM)-based ferromagnetic (FM) materials [1,2] for spintronic device applications. It has been known for a long time, according to the Stoner criterion [3], that the origin of FM order in a conductor arises from the partially occupied (localized) d or f orbitals, which gives rise to a significantly large density of state (DOS) at the Fermi level (E_F), and drives the system into a FM ground state. A half metal [4,5], with a 100% spin-polarized FM state, i.e., conducting in one spin channel and insulating in the other, is an ideal candidate [6] for spin injection and filtering. However, half metals are very rare and only three-dimensional (3D) Heusler compounds [7,8], binary metal oxides CrO_2 [9], and mixed-valence perovskites [10] have been identified as half metals in experiments.

Unfortunately, the strong spin scattering induced by the large spin-orbit coupling (SOC) of heavy elements may significantly reduce the spin-relaxation time and mean free path during spin transport. As a result, great attention has been attracted to searching for sp-electron magnetism in place of d- or f-electron magnetism. Local FM order and even a half-metallic state have been predicted and confirmed to exist in graphene-related 2D systems, some involving local defects or impurities [11–17]. However, the realization of local magnetic states in graphene-related systems requires either large external electric fields or well-ordered defects/dopants. It is therefore highly desirable to discover new mechanisms for realizing delocalized FM states in sp-electron systems beyond the graphene models.

In this paper, we demonstrate a concept for designing homogenous and long-range magnetism in an sp-electron molecular crystal. Our design principle is twofold: first, beyond atomic crystals, molecular crystals are proposed to form with predefined lattice symmetries by taking the advantages of chemical synthesis and epitaxial growth [18–23]; second, overcoming the fixed orbital energy sequence of atomic orbitals (AOs), molecular orbitals (MOs) having different orbital energy and sequences are designed to have artificial frontier orbitals with large angular momenta (e.g., d and f) in a given crystal field to exhibit exotic quantum features, including magnetism [24].

Specifically, we illustrate this design concept by first-principles and model calculations which show the existence of a half-metallic Dirac semimetal state in 2D molecular crystals made of fullerenes. Once these "superatoms" are arranged into a hexagonal lattice, our first-principles calculations show that the frontier f MOs form bare and flat-band-sandwiched (FBS) Dirac bands around the band gap of the 2D C_{20} layer, respectively. More interestingly, additional fractional charge doping induces a spontaneous spin polarization of FBS Dirac bands, giving rise to a half-metallic Dirac semimetal state. For potential device applications, the mechanism of our findings can be applied to design a spin field effect transistor (SFET) built from the 2D C_{20} layer to generate and transport 100% spin-polarized carriers.

II. CALCULATION METHODS

All of the first-principles density functional theory (DFT) calculations are performed using the plane-wave basis Vienna *ab initio* simulation package (VASP) [25,26] with the

*bing.huang@csrc.ac.cn
†fliu@eng.utah.edu

Perdew-Burke-Ernzerhof exchange correlation functional [27]. The cutoff energy for the plane wave is chosen to be 400 eV and the vacuum space is set to 15 Å. All of the atoms in the unit cell are relaxed until the forces are smaller than 0.01 eV/Å. Phonon spectra are obtained using the PHONOPY code [28], where the force constants in real space are also calculated by VASP based on the density functional perturbation theory (DFPT) [29]. Our test calculations show that SOC has a negligible effect on the electronic properties of C_{20} systems. The DFT results are used as input to construct the maximally localized Wannier functions (MLWFs) with the WANNIER90 code [30]. The MOs of a single C_{20} molecule are calculated using the GAUSSIAN09 package [31] at the b3lyp/6-31g level. The charge conductance of the 2D C_{20} layer is calculated using the DFT nonequilibrium Green's function method, as implemented in the ATOMISTIX TOOLKIT (ATK) package [32].

III. RESULTS AND DISCUSSION

The C_{20} molecule, which was first synthesized in 2000 [33], is known as the smallest fullerene and it has a dodecahedral cage structure. Important for our purpose, C_{20} molecules can form molecular crystals with various structural symmetries, such as hexagonal and fcc crystals [19,20]. When C_{20} molecules are constrained into a 2D lattice, e.g., epitaxial growth on a suitable substrate, our extensive structural searches based on DFT total-energy calculations confirm that the hexagonal lattice is the most stable one, as shown in Fig. 1(a). In this structure, two single C-C bonds ($d_1 = 1.53$ Å) between the neighboring C_{20} molecules are formed. The calculated equilibrium lattice constant is $a = 9.89$ Å and thickness $d_2 = 3.94$ Å. The calculated phonon spectra, as shown in Fig. 1(b), further confirms that the 2D C_{20} monolayer is dynamically stable without any imaginary frequencies.

Figure 1(c) shows the calculated band structure of a 2D C_{20} lattice. It is a nonmagnetic (NM) semiconductor with

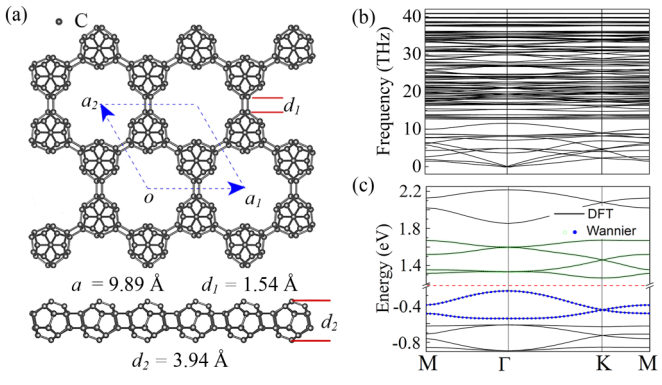

FIG. 1. (a) Top (upper) and side (bottom) views of C_{20} superatomic honeycomb lattices. The blue dashed frame indicates the unit cell, along with the marked unit vectors a_1 and a_2. d_1 defines the distance between two neighboring C_{20} molecules and d_2 defines the thickness of a 2D C_{20} layer. (b) The DFPT-calculated phonon spectra of 2D C_{20}. (c) The DFT-calculated band structure of a 2D C_{20} layer. The WLMF-fitted bare and FBS Dirac bands, marked as dashed lines, are also plotted for comparison. The E_F is marked by the red dashed line.

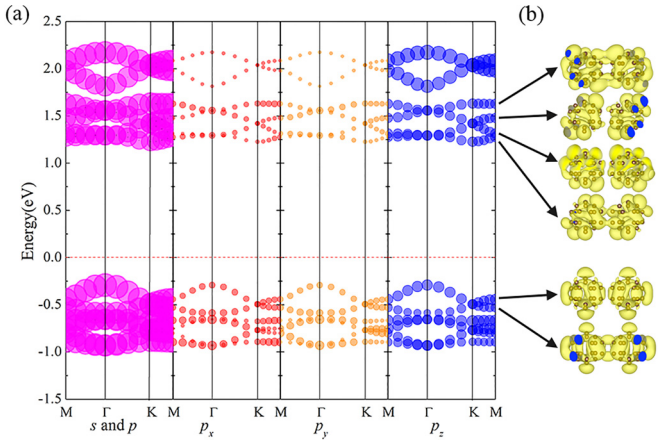

FIG. 2. (a) The DFT-calculated nonmagnetic (NM) electronic energy bands, which are projected onto the s (black), p (pink), p_x (red), p_y (orange), and p_z (blue) orbitals, respectively. The bubble size indicates the weight of the corresponding atomic orbitals contributing to the bands. (b) The NM partial charge density plot at the Γ point for these Dirac bands around the band gap.

an indirect band gap of 1.5 eV. Two subsets of bare Dirac bands and two subsets of FBS Dirac bands appear around the band gap. These Dirac bands appear in different energy ranges without overlapping, and E_F lies in the gap between two sets of bare and FBS Dirac bands. As we learned from graphene models, the appearance of bare (FBS) Dirac bands could be a result of single p_z (double $p_x + p_y$) orbital hopping on a hexagonal lattice [34–37]. However, in our C_{20} system, all the sp AOs from 40 C atoms (per unit cell) contribute to the formation of these Dirac bands and flat bands, as shown in Fig. 2(a). It is found that there is no significant difference between the three p AOs in the weighting factors to form these Dirac bands. Furthermore, the DFT-calculated partial charge distributions around the band edges indicate that the p AOs, shown in Fig. 2(b), are homogenously contributed by all the carbon atoms. Therefore, it is impossible to understand these Dirac bands by the simple single- or double-AO hopping mechanism developed in graphene models.

An individual C_{20} "superatom" has a I_h symmetry in its gas phase (C_{20}^{+2}), and its MOs are arranged in the order of $1s^2 2p^6 3d^{10} 4f^{14} 5g^{18} 6h^{10} 2s^2 3p^6 4d^{10} 5f^2$ [38] based on GAUSSIAN09 calculations, as shown in Fig. 3, which is

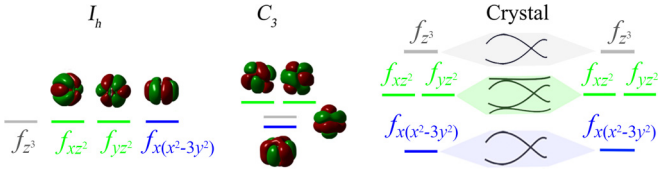

FIG. 3. Schematic illustration of the mechanism for the formation of bare (FBS) Dirac bands. From left to right: the frontier f MOs of an individual C_{20} molecule with I_h (left) and C_3 (middle) symmetries calculated by the GAUSSIAN09 package, and the bare and FBS Dirac bands from single and double f MOs in the 2D C_{20} crystal (right), respectively.

significantly different from that of a single C atom. Based on electron counting, the four degenerated highest occupied MOs (HOMOs) are of the $5f$ type and occupied by two electrons, as shown in the left panel of Fig. 3. When C_{20} molecules are arranged into a hexagonal lattice, these $5f$ MOs are split into two single f_{z^3} and $f_{x(x^2-3y^2)}$ orbitals plus one double-degenerated $f_{xz^2}+f_{yz^2}$ orbital according to C_3 crystal field symmetry, as shown in the middle panel of Fig. 3. From orbital symmetry analysis, one finds that the f_{z^3} or $f_{x(x^2-3y^2)}$ ($f_{xz^2}+f_{yz^2}$) orbital has a similar in-plane symmetry as the $p_z(p_x+p_y)$ orbital in a hexagonal lattice. It is, therefore, reasonable to expect that hopping between f_{z^3} or $f_{x(x^2-3y^2)}$ ($f_{xz^2}+f_{yz^2}$) orbitals will share similar features (bare or FBS Dirac bands shown in the right panel of Fig. 3) as that of p_z (p_x+p_y) orbitals.

Indeed, our Wannier function calculations show that one (two) MLWF orbital(s) of f_{z^3} or $f_{x(x^2-3y^2)}$ ($f_{xz^2}+f_{yz^2}$), located at the center of the carbon cage, can be uniquely applied to perfectly fit the bare (FBS) Dirac bands around the E_F, confirming our physical intuition [green circles and blue dots in Fig. 1(c)]. In order to have a more general understanding of the formation of bare and FBS f-orbital Dirac bands, as discovered in the 2D C_{20} layer, we further develop a single- and double-MO hopping mechanism based on a nearest-neighbor (NN) hopping tight-binding (TB) model, as shown in Fig. 4. Here, the general set of f-orbital-based Slater-Koster hopping integrals [39] are adopted, and a 2×2 (4×4) matrix is constructed to describe the two-band (four-band) single (double) f_{z^3} or $f_{x(x^2-3y^2)}$ ($f_{xz^2}+f_{yz^2}$) orbital hopping in a hexagonal lattice, which can be written as

$$H=\begin{pmatrix} E_1 & T \\ T^* & E_2 \end{pmatrix}. \tag{1}$$

For simplicity, the on-site energies are set to zero ($E_1=E_2=0$) and the off-diagonal terms capture the NN hoppings. For the f_{z^3} single-orbital case [$f_{x(x^2-3y^2)}$ is similar to f_{z^3}], the hopping integral can be described as $T=\xi(\eta+\xi^{-3}e^{iky\pi})[\frac{3}{8}(ff\pi)+\frac{5}{8}(ff\phi)]$. For the $f_{xz^2}+f_{yz^2}$ double-orbital case, the hopping integrals can be described as

$$T=\begin{pmatrix} T_{11} & T_{12} \\ T_{12} & T_{22} \end{pmatrix}, \tag{2}$$

where $T_{11}=\frac{1}{64}[6(4\xi^{-2}+\xi\eta)(ff\sigma)+3\xi\eta(ff\pi)+10(4\xi^{-2}+\xi\eta)(ff\delta)+45\xi\eta(ff\phi)]$, $T_{22}=\frac{1}{64}[18\xi\eta(ff\sigma)+(4\xi^{-2}+\xi\eta)(ff\pi)+30\xi\eta(ff\phi)+15(4\xi^{-2}+\xi\eta)(ff\phi)]$, and $T_{12}=-\frac{\sqrt{3}}{64}\xi\nu[6(ff\sigma)-(ff\pi)+10(ff\delta)-15(ff\phi)]$. Here, $\xi=e^{-ik_x\pi/\sqrt{3}}$, $\eta=e^{ik_y\pi}+e^{-ik_y\pi}$, and $\nu=e^{ik_y\pi}-e^{-ik_y\pi}$. Because the f-orbital angular momentum has $j=4$, we have four basic hopping terms, i.e., $(ff\sigma)$, $(ff\pi)$, $(ff\delta)$, and $(ff\phi)$. In our calculation, the values of these four hopping terms are set to $(ff\sigma)=1.0$, $(ff\pi)=-0.7$, $(ff\delta)=0.03$, and $(ff\phi)=-0.02$ (in unit of t_0), respectively. After the diagonalization of Eq. (1), we obtain two-band and four-band band structures, respectively, as shown in Figs. 4(a) and 4(b) (right panels). Our simple TB models can faithfully reproduce both bare and FBS Dirac bands as obtained from DFT calculations [Fig. 1(c)]. The main features of bare and FBS Dirac bands are insensitive to the detailed values of hopping parameters (except for the slight variation of band dispersion and widths), indicating that they are very robust and generally exist in many f-orbital systems with similar lattice symmetry.

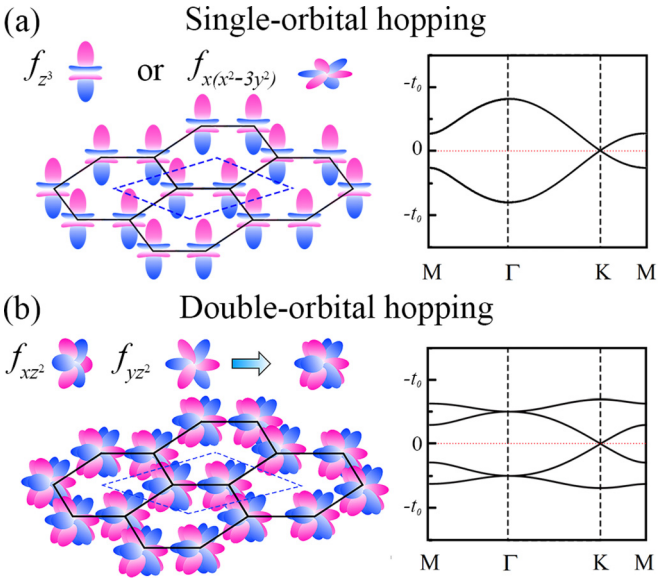

FIG. 4. f-orbital tight-binding Dirac bands: (a) Left panel: schematic picture of f_{z^3} or $f_{x(x^2-3y^2)}$ single-orbital hopping mechanism in a hexagonal lattice. Right panel: the corresponding tight-binding calculated two-band band structure. (b) Left panel: schematic picture of $f_{xz^2}+f_{yz^2}$ double-orbital hopping mechanism in a hexagonal lattice. Right panel: the corresponding tight-binding calculated four-band band structure. All of the parameters are described in the text.

It is important to note that the nontrivial flat band created in the 2D C_{20} layer (wave function is delocalized in real space) is significantly different from that created by defects in semiconductors (wave function is localized in real space) [40]. This unusual flat band at the bottom of the conduction band indicates that a small perturbation of exchange interaction introduced by carrier (electron) doping can induce a large spin splitting because of the very nature of a flat band with an "infinitely" large DOS [40]. Accordingly, the critical value of carrier concentration (n_e) for spontaneous spin polarization in a 2D C_{20} system may be much smaller than that in conventional FM materials, according to the Stoner criterion. To confirm this expectation, we have calculated the magnetic moment of the system as a function of n_e and the spin-polarization energy (the energy difference between a spin-polarized ground state and spin-unpolarized state), which is shown in Fig. 5(a). When n_e increases, the flat band becomes partially occupied and the DOS at E_F increases quickly. The critical n_e for spin polarization in the 2D C_{20} lattice is estimated to be as small as $\sim 2.4\times 10^{12}$ cm^{-2}, marked by a red "A" in Fig. 5(a), which could be achieved in the current experiments by gating (order of 10^{14} cm^{-2}) [41,42]. When $n_e > 2.4\times 10^{12}$ cm^{-2}, the magnetic moment (black circles) continues to increase with the increasing n_e, while the spin-polarization energy decreases (blue triangles). Once

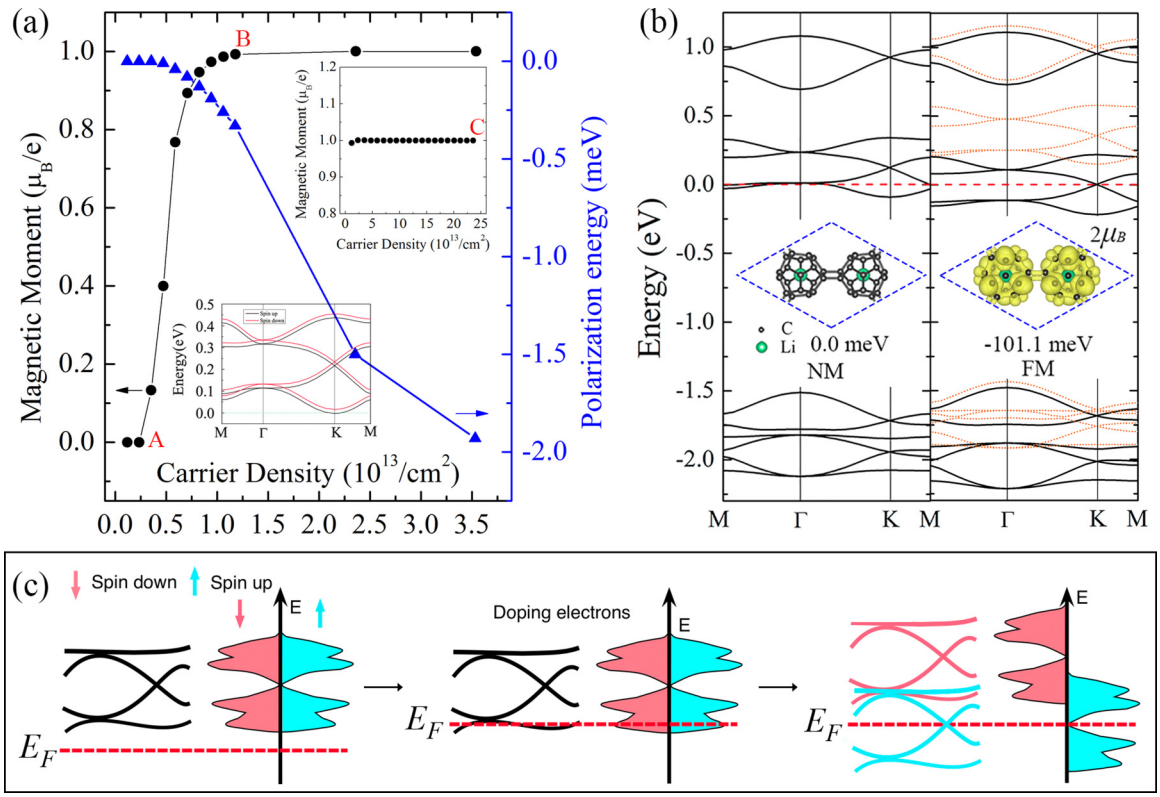

FIG. 5. (a) The calculated magnetic moment and spin-polarization energy of a 2D C_{20} layer as a function of doped carrier (electron) density. From left to right indicate the critical points for the spin-polarized (red "A"), half-metallic (red "B"), and half-metallic Dirac semimetal (red "C") states. Upper inset: the magnetic moment at higher electron concentrations. Lower inset: The DFT-calculated half-metallic band structure of a 2D C20 layer doped with 0.1 electron/unit cell. The black and red lines indicate spin-up and -down bands, respectively. The green dashed line is the Fermi level that is set to zero. (b) The calculated band structures of a 2D Li@C_{20} layer for NM (left panel) and FM (right panel) states, respectively. The spin-up and spin-down bands are represented by the (black) solid and (orange) dotted lines, respectively. The E_F is marked by the red dashed line. Inset in left panel: top view of the 2D Li@C_{20} layer. Inset in right panel: the calculated spin density distribution of the 2D Li@C_{20} layer in its FM state. (c) Illustration of the mechanism for the formation of a half-metallic semimetal state. From left to right: the semiconducting electronic structure of a 2D C_{20} layer, the partially filled flat-band state due to electron doping, and the half-metallic semimetal state mediated by doping of flat bands.

$n_e > 1.18 \times 10^{13}$ cm^{-2}, marked by a red "B" in Fig. 5(a), the magnetic moment saturates at 1.0 μ_B/e, as shown in the upper and lower insets of Fig. 5(a), and the system becomes a half metal, and the corresponding band structure is shown, respectively.

Another effective approach to doping of a C_{20} molecule is to encapsulate alkali atoms into the cage of fullerene, which has been achieved in the experiments [43,44]. Taking Li as a prototypical example, we insert one Li atom into each C_{20} cage to form a 2D Li@C_{20} layer, as shown in the inset of Fig. 5(b). Overall, the equilibrium geometry and lattice parameters of the 2D C_{20} layer change very little after Li doping. When spin polarization is excluded (NM case), the calculated band structure is almost the same as the undoped case, except for the shift of E_F to the contacting region between the Dirac bands and the flat band. Including spin polarization, the half-metallic ground state [right panel of Fig. 5(b)] is energetically more favorable than the NM and antiferromagnetic states by about 101.1 and 89.0 meV per unit cell, respectively. Interestingly, the E_F locates exactly at the Dirac point of the majority (spin-up) channel, creating a half-metallic Dirac semimetal phase with a ~0.2 eV half-metallic gap, and the n_e is ~2.3×10^{14} cm^{-2}, marked by a red "C" in the upper inset of Fig. 5(a). The Fermi velocity of 2D Li@C_{20} is estimated to be 1.05×10^5 m/s, close to that of graphene.

The above findings demonstrate an attractive mechanism for realizing a half-metallic Dirac semimetal state by manipulating the MOs of fullerene. First, a C_{20} molecule, which has degenerate 5f MOs at HOMO, can be used to generate FBS Dirac bands at the bottom of the conduction band under specific crystal field splitting [left panel of Fig. 5(c)]. Second, small "finite" (fractional) charge doping of the flat band will induce an "infinitely" large DOS at E_F and drive the system into a partially filled flat-band state. According to the Stoner criterion, a large spin polarization is induced to reduce the instability. As a result, the system is converted from a NM [middle panel of Fig. 5(c)] to a half-metallic [right panel of Fig. 5(c)] ground state. In particular, a half-metallic Dirac fermion state can be achieved by a critical n_e by gating or monolayer decoration of alkali atoms.

In practice, the growth of a fullerene monolayer with controllable lattice symmetries could be achieved by the selection of specific substrates [19,20]. Hexagonal BN (h-BN) has been widely selected as an ideal substrate to grow various 2D materials by van de Waals (vdW) epitaxy. Using h-BN as a candidate substrate, our structure search shows that 1 × 1 2D

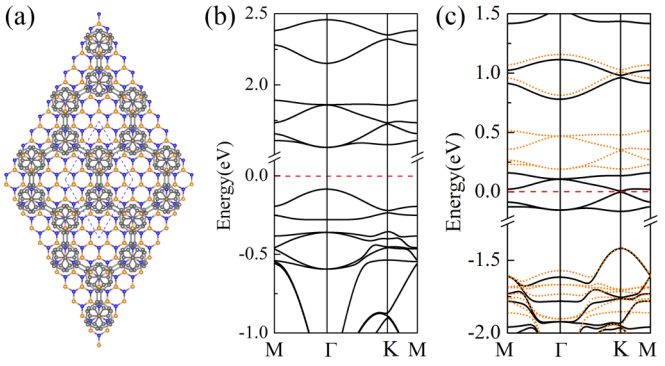

FIG. 6. (a) Top view of the 2D C_{20} honeycomb lattice on the monolayer h-BN substrate. Blue and orange beads are the N and B atoms, respectively. Li and C atoms are still represented by green and gray beads, respectively. (b) Calculated band structure of 2D C_{20} on the h-BN substrate. (c) The calculated spin-polarized band structure of 2D Li@C_{20} on the h-BN substrate. The spin-up and spin-down bands are represented by the black solid and orange dotted lines, respectively. The E_F is marked by the red dashed line.

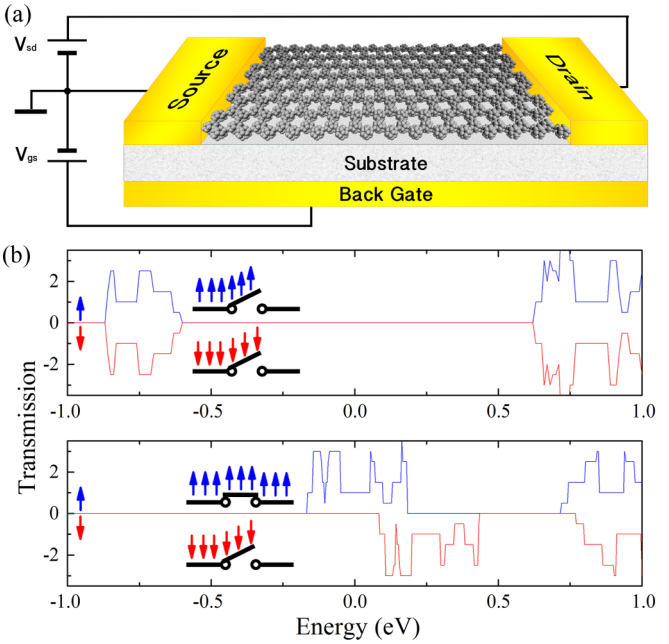

FIG. 7. (a) The schematic device model of 2D C_{20} SFET. (b) From top to bottom: the calculated spin-polarized charge conductances for a zero (OFFstatus) and a nonzero critical (ON status) V_{gs}, respectively. The E_F is set to zero.

C_{20} (or 2D Li@C_{20}) can perfectly fit a 4×4 h-BN supercell (lattice mismatch is smaller than 1%), as shown in Fig. 6(a). Combining the vdW corrections with DFT, the optimized structure of 2D C_{20} on h-BN is shown in Fig. 6(a) (the structure of 2D Li@C_{20} on h-BN is similar and not shown here). The minimal distance between C_{20} and the h-BN is around 3.2 Å, indicating a weak interfacial interaction. Our band structure calculations have confirmed that the basic electronic structural characteristics of 2D C_{20} [f-orbital Dirac bands around the bottom of the conduction band and the top of the valence band, as shown in Fig. 6(b)] and 2D Li@C_{20} [half-metallic Dirac band across the Fermi level, as shown in Fig. 6(c)] maintain on the h-BN substrate. Besides h-BN, it is expected that 2D C_{20} could also be grown on other insulating substrates where its exciting electronic structures can be maintained.

Once the hexagonal lattice of the C_{20} monolayer is grown on an insulating substrate with weak interaction, e.g., the case of C_{20} on h-BN, then a 2D C_{20}-based SFET model device can be made, as shown in Fig. 7(a). Without gate voltage ($V_{gs} = 0$), the 2D C_{20} monolayer is NM semiconducting with a band gap of ∼1.5 eV. Thus, a conductance gap exists around the E_F (OFF status), as shown in Fig. 7(b) (upper panel). To overcome this transport gap, a bias voltage $V_{sd} \geqslant 1.5$ V has to be applied to drive the spin-unpolarized charge flow through the 2D C_{20} layer. When the V_{gs} is applied larger than a threshold to achieve the critical doping to occupy the conduction flat band, the system is converted into a half-metallic state (ON status), as shown in Fig. 7(b) (bottom panel). In this configuration, a small V_{sd} is able to drive a 100% spin-polarized current through the 2D C_{20} monolayer. Furthermore, a proper V_{gs}-induced charge doping can convert the system into a half-metallic Dirac semimetal state, in which the carriers with 100% spin polarization will transport with ultrafast speed.

IV. CONCLUSION

In summary, we demonstrate a mechanism for achieving a half-metallic Dirac semimetal state from the manipulation of MOs of fullerenes, by designing large-angular-momentum (d and f) frontier MOs from linear combination of small-angular-momentum (s and p) AOs. Our discovery opens an avenue to realizing exotic quantum states from orbital-designed molecular crystal lattices.

ACKNOWLEDGMENTS

B.C. acknowledges the support from NSFC (Grant No. 11404188) and China Scholarship Council (Grant No. 201406225022). B.H., K.-H.J., W.J., and F.L. acknowledge the support from the U.S. DOE-BES (Grant No. DE-FG02-04ER46148). B.H. also acknowledges the support from NSFC (Grant No. 11574024) and NSAF (Grant No. U1530401). We thank the CHPC at the University of Utah for providing the computing resources.

[1] T. Dietl and H. Ohno, Rev. Mod. Phys. **86**, 187 (2014).
[2] S. A. Wolf, Science **294**, 1488 (2001).
[3] E. C. Stoner, Proc. R. Soc. London, Ser. A **165**, 372 (1938).
[4] R. A. de Groot, F. M. Mueller, P. G. van Engen, and K. H. J. Buschow, Phys. Rev. Lett. **50**, 2024 (1983).
[5] H. van Leuken and R. A. de Groot, Phys. Rev. Lett. **74**, 1171 (1995).

[6] F. J. Jedema, A. T. Filip, and B. J. van Wees, Nature (London) **410**, 345 (2001).
[7] J. W. Dong, L. C. Chen, C. J. Palmstrom, R. D. James, and S. McKernan, Appl. Phys. Lett. **75**, 1443 (1999).
[8] M. Jourdan, J. Minár, J. Braun, A. Kronenberg, S. Chadov, B. Balke, A. Gloskovskii, M. Kolbe, H. J. Elmers, G. Schönhense, H. Ebert, C. Felser, and M. Kläui, Nat. Commun. **5**, 3974 (2014).
[9] S. M. Watts, S. Wirth, S. von Molnár, A. Barry, and J. M. D. Coey, Phys. Rev. B **61**, 9621 (2000).
[10] J.-H. Park, E. Vescovo, H.-J. Kim, C. Kwon, R. Ramesh, and T. Venkatesan, Nature (London) **392**, 794 (1998).
[11] M. Fujita, K. Wakabayashi, K. Nakada, and K. Kusakabe, J. Phys. Soc. Japan **65**, 1920 (1996).
[12] H. Hu, Z. Wang, and F. Liu, Nano. Res. Lett. **9**, 690 (2014)
[13] Y.-W. Son, M. L. Cohen, and S. G. Louie, Nature (London) **444**, 347 (2006).
[14] T. B. Martins, R. H. Miwa, A. J. R. da Silva, and A. Fazzio, Phys. Rev. Lett. **98**, 196803 (2007).
[15] E.-j. Kan, Z. Li, J. Yang, and J. G. Hou, J. Am. Chem. Soc. **130**, 4224 (2008).
[16] P. Esquinazi, D. Spemann, R. Höhne, A. Setzer, K.-H. Han, and T. Butz, Phys. Rev. Lett. **91**, 227201 (2003).
[17] G. Z. Magda, X. Jin, I. Hagymasi, P. Vancso, Z. Osvath, P. Nemes-Incze, C. Hwang, L. P. Biro, and L. Tapaszto, Nature (London) **514**, 608 (2014).
[18] N. Stock and S. Biswas, Chem. Rev. **112**, 933 (2012).
[19] Z. Wang, X. Ke, Z. Zhu, F. Zhu, M. Ruan, H. Chen, R. Huang, and L. Zheng, Phys. Lett. A **280**, 351 (2001).
[20] Z. Iqbal, Y. Zhang, H. Grebel, S. Vijayalakshmi, A. Lahamer, G. Benedek, M. Bernasconi, J. Cariboni, I. Spagnolatti, R. Sharma, F. J. Owens, M. E. Kozlov, K. V. Rao, and M. Muhammed, Eur. Phys. J. B **31**, 509 (2003).
[21] X. Roy, C.-H. Lee, A. C. Crowther, C. L. Schenck, T. Besara, R. A. Lalancette, T. Siegrist, P. W. Stephens, L. E. Brus, P. Kim *et al.*, Science **341**, 157 (2013).
[22] J. Plas, O. Ivasenko, N. Martsinovich, M. Lackinger, and S. De Feyter, Chem. Commun. **52**, 68 (2016).
[23] L. A. Rochford, T. S. Jones, and C. B. Nielsen, J. Phys. Chem. Lett. **7**, 3487 (2016).
[24] D. A. Tomalia and S. N. Khanna, Chem. Rev. **116**, 2705 (2016).
[25] G. Kresse and J. Furthmüller, Comput. Mater. Sci. **6**, 15 (1996).
[26] G. Kresse and J. Furthmüller, Phys. Rev. B **54**, 11169 (1996).
[27] J. P. Perdew, K. Burke, and M. Ernzerhof, Phys. Rev. Lett. **77**, 3865 (1996).
[28] A. Togo and I. Tanaka, Scr. Mater. **108**, 1 (2015).
[29] X. Gonze and C. Lee, Phys. Rev. B **55**, 10355 (1997)
[30] A. A. Mostofi, J. R. Yates, Y. S. Lee, I. Souza, D. Vanderbilt, and N. Marzari, Comput. Phys. Commun. **178**, 685 (2008).
[31] M. J. Frisch *et al.*, Computer code GAUSSIAN09, Rev. C.01 (Gaussian, Inc., Wallingford, CT, 2009).
[32] http://quantumwise.com
[33] H. Prinzbach, A. Weiler, P. Landenberger, F. Wahl, J. Worth, L. T. Scott, M. Gelmont, D. Olevano, and B. v. Issendorff, Nature (London) **407**, 60 (2000).
[34] P. R. Wallace, Phys. Rev. **71**, 622 (1947).
[35] S. Reich, J. Maultzsch, C. Thomsen, and P. Ordejón, Phys. Rev. B **66**, 035412 (2002).
[36] C. Wu, D. Bergman, L. Balents, and S. Das Sarma, Phys. Rev. Lett. **99**, 070401 (2007).
[37] Z. Liu, Z.-F. Wang, J.-W. Mei, Y.-S. Wu, and F. Liu, Phys. Rev. Lett. **110**, 106804 (2013).
[38] A. V. Verkhovtsev, R. G. Polozkov, V. K. Ivanov, A. V. Korol, and A. V. Solov'yov, J. Phys. B At. Mol. Opt. Phys. **45**, 215101 (2012).
[39] J. C. Slater and G. F. Koster, Phys. Rev. **94**, 1498 (1954).
[40] Z. Liu, F. Liu, and Y.-S. Wu, Chinese Phys. B **23**, 077308 (2014).
[41] B. Radisavljevic, A. Radenovic, J. Brivio, V. Giacometti, and A. Kis, Nat. Nanotechnol. **6**, 147 (2011).
[42] T. Roy, M. Tosun, X. Cao, H. Fang, D.-H. Lien, P. Zhao, Y.-Z. Chen, Y.-L. Chueh, J. Guo, and A. Javey, ACS Nano **9**, 2071 (2015).
[43] J. R. Heath, S. C. O'Brien, Q. Zhang, Y. Liu, R. F. Curl, F. K. Tittel, and R. E. Smalley, J. Am. Chem. Soc. **107**, 7779 (1985).
[44] S. Aoyagi, E. Nishibori, H. Sawa, K. Sugimoto, M. Takata, Y. Miyata, R. Kitaura, H. Shinohara, H. Okada, T. Sakai, Y. Ono, K. Kawachi, K. Yokoo, S. Ono, K. Omote, Y. Kasama, S. Ishikawa, T. Komuro, and H. Tobita, Nat. Chem. **2**, 678 (2010).